# 3D tomographic reconstruction of irregular rough particles from interferometric images

Barbara Delestre, Alexis Abad, Mohamed Talbi, Michael Fromager, Marc Brunel

Version of Record: https://www.sciencedirect.com/science/article/pii/S0022407322001285
Manuscript_442db57a86b82b1c30d0bed84ade48f8

# 3D tomographic reconstruction of irregular rough particles from interferometric images

Barbara Delestre[1,*], Alexis Abad[1], Mohamed Talbi[1], Michael Fromager[2] Marc Brunel[1],

[1]*UMR CNRS 6614 CORIA, Université de Rouen Normandie, Avenue de l'Université, BP 12, 76801 Saint-Etienne du Rouvray Cedex, France*
[2]*UMR CNRS 6252 CIMAP, CEA, Ensicaen, Université de Caen, 6 Bd Maréchal Juin, F-14050 Caen Cedex, France*
*delestrb@coria.fr

**Abstract**
Using a Digital Micromirror Device (DMD), the 3D-reconstruction of programmable rough particles (centrosymmetric or non-centrosymmetric) are done from a set of 120 interferometric images. This can be done using the error-reduction (ER) algorithm for the 2D shape reconstructions and the filtered back-projection for the 3D tomographic reconstruction.
*Keywords: Interferometric particle imaging, Speckle, Error-reduction algorithm, Filtered back-projection, 3D tomographic reconstruction*

## 1. Introduction

The tomography of irregular rough particles in a flow is particularly interesting in domains such as meteorology, biology, health, combustion and other concerned. In many domains a single-shot technique that permit to "freeze" the particles on a sensor. A short light pulse is necessary because particles can reach important speed in a flow. For example in airbone operation or in icing wind tunnels, the relative speed of the particles as ice crystals or ashes due to the plane's flight can exceed 200 $m.s^{-1}$. In addition, an instrument should ideally tend to real-time analysis. A configuration as a CT scan [1-5] (computed tomography scan) in medicine where the object is fixed while the x-ray tube rotates around the object is not applicable. A setup where the particle is illuminated by a unique short flash, while different sensors acquire simultaneously the signal delivered by the particle in different directions, must be envisaged. Techniques based on light scattering properties are interesting and in this family interferometric particle imaging [6-11] seems promising.

When illuminated by a laser pulse, particles scatter light. Using an out-of-focus imaging set-up, the images of irregular rough particles are speckle patterns. The difficulty of the study lies in the nature of these interferometric out-of-focus images. After 2D-Fourier transformation, these images give the 2D-autocorrelation of the contour of the particle projected in the plane of the CCD sensor (corresponding to this angle of view), and not the contour of the particle itself. These results have been validated in several experimental cases [12-18].

In a previous study, we have shown that the 3D-reconstruction of a particle can then be done from a set of three simulated interferometric images of this particle (from three perpendicular angles of view). As the 2D-autocorrelation of a 2D-shape does not give the 2D-shape of an object itself, each interferogram is analyzed using a phase-retrieval algorithm: the error-reduction (ER) algorithm which enables to obtain a function $\boldsymbol{f}(\boldsymbol{x}, \boldsymbol{y})$ from measurements that give the modulus of its 2D-Fourier transform $|\boldsymbol{F}(\boldsymbol{u}, \boldsymbol{v})|$ by reconstructing the phase of the 2D-Fourier transform. The method has been tested on irregular rough particles programmed with a DMD and it shows great potentiality.

To obtain a better estimate of the 3D-shape, it is necessary to reconstruct with more precision the 3D-contour of the particle by adding new angles of view. However, the major difficulty in adding viewing angles is the rear projection of the reconstructed 2D projections at different angles. The three-dimensional shape and volume of a particle is estimated using tomographic reconstruction algorithms from the acquired projections.

It is well known that CT-scans in medicine acquire more than 100 angles of views to perform a high-accuracy tomography of the patients. In this paper, we study whether a configuration where many CCD sensors would be located around particles in a flow can be applied to perform a high-accuracy tomography of the particles using interferometric imaging. The set-up under consideration is represented on figure 1 in the case of eight angles of view regularly separated from each other.

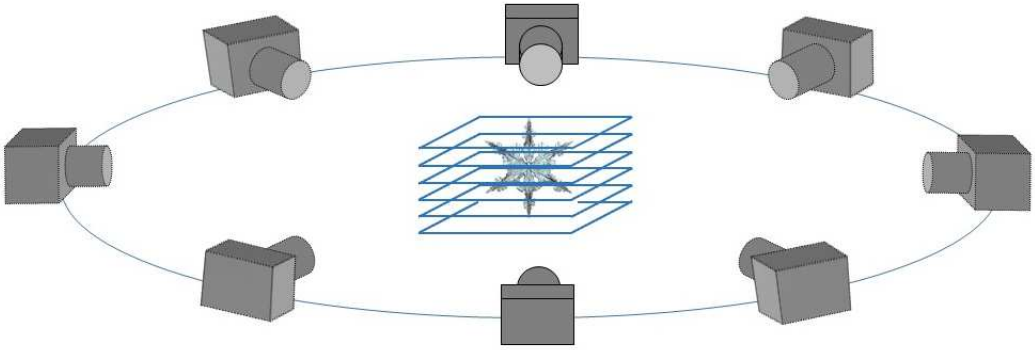

Fig. 1. Experimental configuration under study in this article: irregular rough particles are observed simultaneously from different angles of view regularly separated from each other (8 cameras on this figure).

We will actually identify how many sensors would be necessary to obtain accurate 3D-reconstructions of the particles. Experimentally, this study will be done using a specific set-up based on the use of a Digital Micromirror Device (DMD): a rough particle is programmed on a DMD. It is illuminated by a laser beam. A defocused imaging system records the scattered pattern, that reproduces the interferometric image of an irregular rough particle. Section 2 will describe the experimental set-up used to record the interferometric images of ‘‘programmed’’ rough particles, using the DMD [6,19]. In section 3, the interferometric images of a ‘‘programmable’’ particle, observed from 120 angles of view separated by 3 degrees from each other, will be presented and a 2D-reconstruction of each view, using the error-reduction algorithm, will be performed. Section 4 will propose a short theoretical part of the tomography reconstruction that has been developed to realize the 3D-reconstruction of particles. Section 5 will present the tomography reconstruction with only 8 angles of view of a “programmed” particle and a comparison with a 3D reconstruction of this particle performed with 120 angles of view. The figure 2 summarizes these different steps that will be done and explained in the next sections.

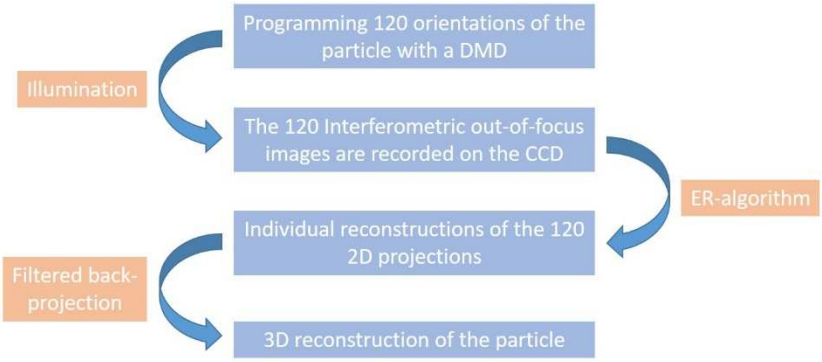


Fig. 2 : Diagram of the steps of the 3D reconstruction of a particle programmed with the DMD (in the case of 120 angles of view).

## 2. Experimental setup and image acquisition

It is not possible experimentally to generate a flow with irregular particles whose orientation is perfectly known. We can eventually know the exact shape of the particles that are injected into a flow, but we are not able to predict their exact orientation when they reach the field of view of an imaging set-up. It is thus not possible to test rigorously tomographic reconstructions of perfectly known rough particles (in size, shape and orientation). In this study, we have decided to record the interferometric images of perfectly known ‘‘programmable’’ particles. To do it, figure 3 shows the set-up used. It is composed of a Digital Micromirror Device (DMD) that reproduces a ‘‘programmed” rough particle’ illuminated by an HeNe laser (wavelength: 632.8 nm). The telescope is the

association of a (× 10) microscope objective and a classical lens (focus length 10cm). It enlarges the beam emitted by the laser to cover the whole surface of the DMD. With the DMD, the particles created are fixed. It is thus not necessary to use a pulsed laser. A CW HeNe laser is preferred to illuminate the DMD and generate the pattern, because it allows a better protection of the micromirror device. The DMD is composed of many pivoting micromirrors (1920 × 1080 mirrors with a square geometry). The separation between the centers of two adjacent mirrors is 7.56 µm. Each micromirror has two possible states ("on" and "off"), which correspond to two inclinations (12° angle). The size of the whole DMD is 1.4 cm × 0.8 cm. The particle is composed of the micromirrors that are programmed ''on-state'', i.e. that reflect the laser light into the direction of an imaging system. Other micromirrors keep ''off-state'': i.e. no reflection in the direction of the imaging system. This imaging system is composed of a lens and a CCD sensor. The lens (L3) of Fig.3. is a Nikon objective of focus length f=180 mm. Fig.3 is not at the real scale. In the set up used $z_1$=42 cm and $z_2$=37,8 cm (using extension rings). The CCD sensor records the out-of-focus image of the particle programmed on the DMD, which is a speckle pattern. This CCD sensor is a Thorlabs BC106N-VIS/M camera with 1360 x 1024 pixels, and a pixel size of 6.45 µm×6.45 µm.

Let us now explain the procedure used to reproduce an experiment of tomography with the set-up of Fig. 1. We consider a perfectly known dendrite-like particle whose 3D-shape. This particle is then observed from 120 angles of view, as would be done with a CT-scanner. With our set-up, these 120 angles of view of the particle correspond in practice to 120 orientations of the particle. These 120 orientations are programmed with the DMD. For each angle of view, the particle is composed of a large number of on-state micromirrors. The choice of the on-state micromirrors is done randomly for each view, but they are always located within the contour of the dendrite-like particle, according to the rotation angle for each view. The difference between two successive views is a rotation of the particle of 3° around the X-axis.

For each angle of view (i.e. for each orientation programmed on the DMD) a centered crop of the interferometric image ($Iview\ (x,\ y)$) recorded on the CCD sensor is considered. The size of this crop of the interferometric image is $680 \times 680$ pixels (the pixel size of the CCD sensor is 6.45 µm). The particle's reconstructions will be done from these crops for the 120 interferometric images obtained experimentally.

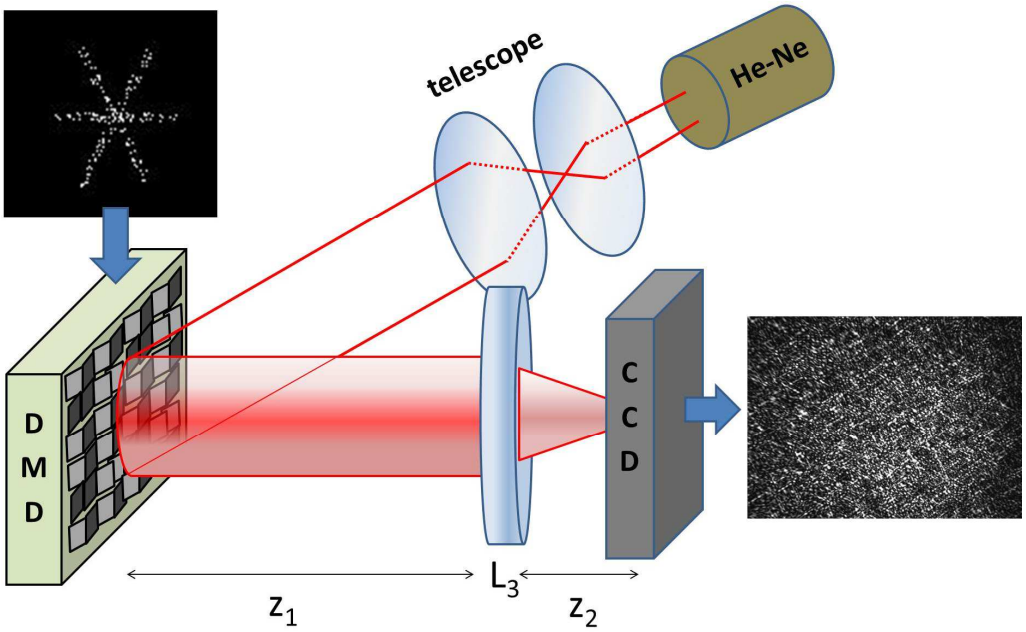


Fig. 3. Experimental set up to generate the interferometric images of « programmable » particles with a Digital Micromirror Device (the speckle pattern recorded with the CCD sensor (right) is associated to the particle programmed on the DMD (left)).

## 3. Individual reconstructions of the 2D-projections

Assuming that irregular rough particles can be assimilated to a set of emitters on the envelope of the particle, it has been shown in [15] that the contour of the projected shape of the particle in the CCD sensor's plane is

related to the 2D-Fourier transform of its interferometric out-of-focus image. This can be described by the following scalar equation (1):

$$|FT_{2D}[I](\lambda\, B_{tot}\, u, \lambda\, B_{tot}\, v)| \propto |A_{2D}[G_0](dx, dy)| \quad (1)$$

Where $I$ is the intensity of the out-of-focus pattern of the particle under laser illumination, and $G_0$ the electric field emitted by the illuminated particle (a sum of Dirac point emitters). $FT_{2D}$ denotes the 2D-Fourier transform, $A_{2D}$ the 2D-autocorrelation. $\lambda$ is the wavelength of the laser. $\lambda B_{tot}$ is the scaling factor between both functions. $B_{tot}$ is obtained from optical ray matrix formalism. During an interferometric particle imaging experiment, the intensity I(x,y) is recorded on the CCD sensor. According to relation (1), its 2D-Fourier transform is then assimilated to the 2D-autocorrelation of the envelope of the particle (for this angle of view). The threshold of the 2D-Fourier transform has been determined manually. But the same threshold is then applied for all particles, and for all orientations programmed with the DMD.

The dendrite-shaped particle that is first considered is depicted on Figure 4. It is made of 2100 point emitters distributed over the entire surface of the particle. It consists of six main branches, each being 567 µm long and 37,8 µm wide, with small secondary branches at their ends. Recent flight missions have shown that clouds with high Ice Water Contents can contain crystals whose size is in the range $400 - 800\ \mu m$ and peak values of up to $2\ mm$ [20]. As the DMD set-up is well adapted to reproduce such dimensions (by addition of many micromirrors whose individual size is $7.56\ \mu m$), this choice of size has been done to carry our experiments. Note that the ER-phase-reconstruction algorithm has been tested and validated in previous studies with similar parameters [21]. Figure 5.a) shows the face of the particle programmed first on the DMD (i.e. the specific orientation when the dendrite is in the (X,Y)-plane), while Fig. 5(b) shows its interferometric image obtained on the CCD sensor. Part (a) of visualization 1 presents then the particle programmed on the DMD, corresponding to 120 angles of view (with a rotation angle of 3° between two successive angles of view). All interferometric images (corresponding to all 120 orientations) recorded on the CCD sensor appear on part (b) of visualization 1, for each orientation of the particle.

Figure 5.c) is the 2D reconstruction of the interferometric out-of-focus image of Fig. 5.b (for this angle of view). The visualization 1 is the stacking of 120 2D-reconstructions for 120 angles of view. After application of the scaling factor $\lambda B_{tot}$ (previously mentioned in Eq. (1)), the pixel size in figure 5.c) is 11 $\mu m$. Quantitatively, the coefficient $B_{tot}$ equals - 0.076 m. The scaling factor is already applied in Fig.5.c). It explains the offset of the origin with the Fig.5.a), because the particle was not centered. But the reconstructed sizes are correct. Let us now briefly recall the iterative phase retrieval algorithm used (the ER-algorithm) [22-24].

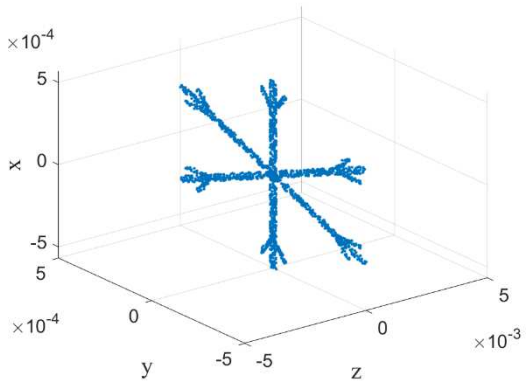


Fig. 4. Three-dimensional representation of the 1134 µm wide dendrite-like particle that will be considered. (All axes in meters)

First step is to create a starting object $g1(x,y)$. For this, a support S, obtained from the tri-intersection [25] of the binarized form of the Fourier transform of the speckle image, is necessary. Let us briefly recall the tri-intersection method that is used to do this. We start from a $2D$ object called $A$. It is duplicated twice and the copy number 1 (resp. 2) is translated from vector $w1$ (resp. 2). The copies of the initial object $A$, translated from $w_1$ and $w_2$ respectively, are called $(A + w_1)$ and $(A + w_2)$ respectively. The origin of the vector $w_1$ is the center of $A$ and this extremity is on the border of $A$. The origin of the vector $w_2$ is the center of $A$ and this extremity is at the intersection of the borders of $A$ and $(A + w_1)$. Finally, the tri-intersection $B$ of the shape $A$ ($B = A \cap (A + w1) \cap (A + w2)$ ) has a 2D autocorrelation that matches the initial object $A$.

Once the support is created, the pixels belonging to this support (white pixels) are replaced by the corresponding pixels in the image of the 2D Fourier transform of the speckle. This shortcut allows converging faster to a solution using the phase of the Fourier transform restricted to the support of the tri-intersection object. The error-reduction algorithm is then an iterative process that leads to the obtention of a good estimate $g_n(x, y)$ of the particle's shape after n iterations. The number of iterations is between 2 and 10. There is little or no evolution beyond this value. More details can be found in reference [21].

The results obtained are summarized on Figure 5(c) and on part (c) of visualization 1. In summary, we have obtained 120 2D-reconstructions of the dendrite-like particle, from its 120 interferometric images, corresponding to observations from 120 different angles of view. Next step is now to proceed to the 3D reconstruction of the 3D-particle from these 120 individual 2D-reconstructions.

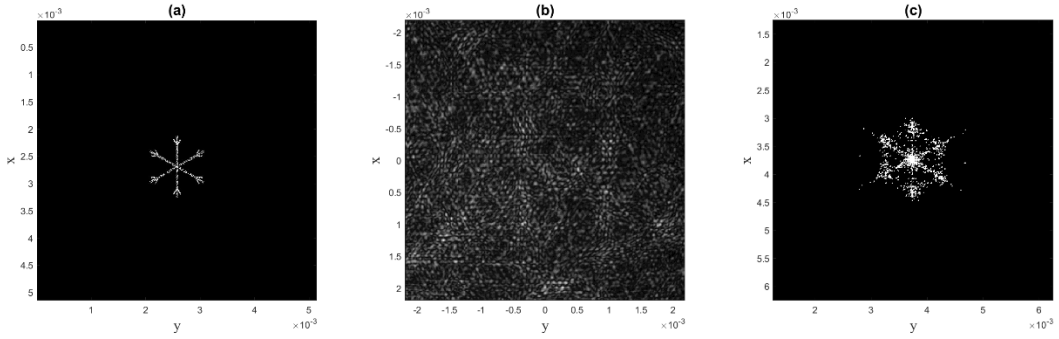


Fig. 5. In a) projection of the particle in the (x,y) plan, in b) the center of the out-of-focus interferometric image, and in c) the 2D-projection reconstructed, (see Visualization 1). (All axes in meters)

## 4. Theory: Tomographic reconstruction

The 3D-reconstruction will be done slice by slice. This is illustrated on figures 1 and 6 where each horizontal plane represents one of these slices. The whole 3D-particle will then be reconstructed stacking these different slices of the reconstructed particle. Let us thus detail the principle of the reconstruction in one slice.

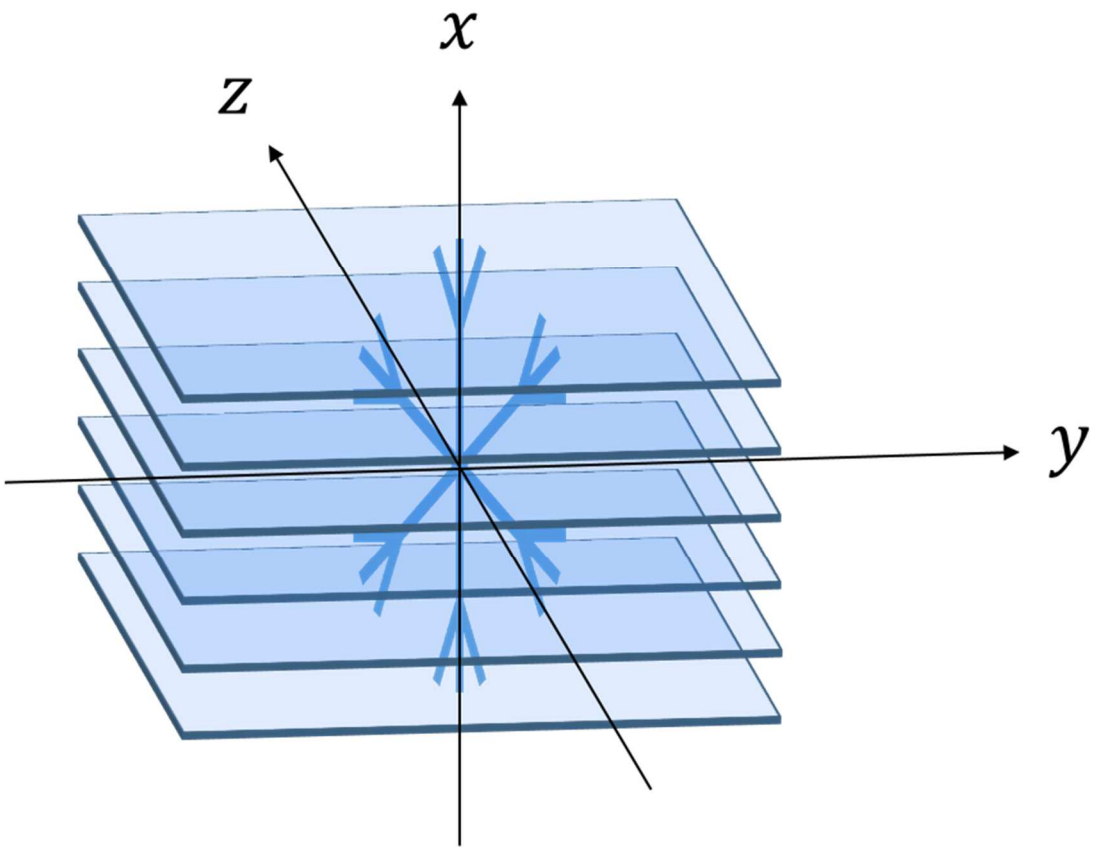


Fig. 6. Illustration of the reconstruction of the 3D-shape of the particle obtained by sequential reconstruction of the parallel sections

*4.1. Introduction to tomographic reconstruction*

The different views correspond to a rotation around axis X (see previous sections 2 and 3). The transverse sections of figure 6 are thus (Y,Z) sections. Consider a section of the particle: we can define the function $f(y,z)$ that represents the particle. It should be equal to zero outside the particle. The camera rotates around the particle. For each rotation angle that has been programmed, the shape's reconstruction from the interferometric image has lead to horizontal projections of this slice of the reconstructed particle. In Figure 7, function $f(y,z)$ is expressed in the fixed Cartesian coordinate system $(O,y,z)$. For the rotation angle $\theta$, the horizontal projection $p_\theta(u)$ of function $f(y,z)$ on the rotating axis u (see figure 5) is expressed as a Radon transform:

$$p_\theta(u) = \int_{-\infty}^{+\infty} f(y,z)\, dv = \int_{-\infty}^{+\infty} f(u\cos(\theta) - v\sin(\theta)\,, u\sin(\theta) + v\cos(\theta))\, dv$$

$$= (\Re_\theta f)(u) \qquad (7)$$

$\Re$ denotes the operator of the radon transform [26,27]. The Radon transform $p_\theta(u)$ of the distribution $f(y,z)$ represents the integral of lines of the values of $f(y,z)$ along the line inclined at an angle $\theta$ with respect to the y-axis.

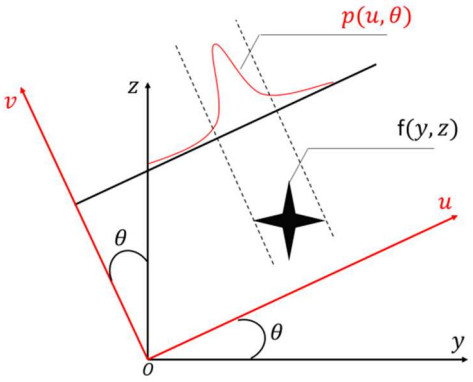


Fig. 7. Projection p(u,θ) de la distribution d'intensité f(y,z) sous l'angle θ

The problem of tomographic reconstruction consists in moving from Radon space to the spatial domain. The Radon transform has to be inverted in order to estimate the object $f(y,z)$ from the projections $p_\theta(u)$ obtained experimentally after reconstruction for each angle $\theta$. Solving the tomographic reconstruction problem consists in obtaining the particle's distribution $f$ by applying the inverse operator of the Radon transform $\Re^{-1}$ to the set of acquired projections:

$$f(y,z) = (\Re^{-1}(\Re_\theta f))(y,z) \qquad (8)$$

In theory, it is necessary to know the continuous projections over the whole interval $[0;\pi]$ $\{p_\theta(u)|\ 0 \leq \theta \leq \pi\}$, which means for all angles $\theta$ in this interval. Experimentally we have used a finite number of angles (120). In addition, the detectors are of finite size, which leads to sampling of the projections. Alternative methods have thus to be used to estimate the inverse Radon transform. They fall into three classes: analytics, algebraic and statistics methods. We will use analytical methods for the reconstruction of the particles.

*4.2. Analytical reconstruction method*

The simplest method to reconstruct an object from its projections is to backproject the value of each projection $p_\theta(u)$ onto the reconstruction plane. For a given angle, the value of $p_\theta(u)$ is assigned to all pixels that lie along the integration line. The image $f^*(y,z)$ obtained after rear projection is not exactly the image sought since it is accompanied by a blur (star artifact) which distorts the result obtained, particularly when the number of angles of view is low. A method that eliminates these star artefacts has then to be used: it uses the Fourier transform of a two-dimensional image. The Fourier central slice theorem [26-28] shows that the Fourier transform $P_\theta(U)$ of a projection $p_\theta(u)$ is equal to the Fourier transform of the image in the central slice perpendicular to the direction of projection, which writes:

$$P_\theta(U) = F\left(U_y = Ucos(\theta), U_z = Usin(\theta)\right) \qquad (10)$$

The central slice theorem [26-28] makes it possible to consider the reconstruction of the tomographic slice directly using an inverse Fourier transform. However, as the number of projections is not infinite, the filling of the frequency plane is often highly incomplete, especially for high frequencies; there are still gaps that must be filled by linear interpolations. This step of filling the Fourier planes is long and complex, which makes this tomographic reconstruction method unattractive and therefore very rarely used.

Filtered back projection [28], that is classically used in scanners and that will be used in this work, is an analytical method derived from the central section theorem. To perform a filtered back projection, it is necessary to transpose the problem into Fourier space. The inverse Fourier transform allows to estimate $f(y,z)$ from $F(U_y,U_z)$ according to:

$$f(y,z) = \int_{-\infty}^{+\infty}\int_{-\infty}^{+\infty} F(U_y,U_z)e^{i2\pi(yU_y+zU_z)}dU_y dU_z \qquad (11)$$

Using the central section theorem (equation 10), we can replace $F(U_y,U_z)$ by the Fourier transform of the projections $P_\theta(U)$:

$$f(y,z) = \int_{-\infty}^{+\infty}\int_{-\infty}^{+\infty} P_\theta(U)e^{i2\pi(yU_y+zU_z)}dU_y dU_z \qquad (12)$$

We then proceed to the transition in polar coordinates. The change to polar coordinates leads to :

$$f(y,z) = \int_{0}^{2\pi}\int_{-\infty}^{+\infty} P_\theta(U)e^{i2\pi U(ycos(\theta)+zsin(\theta))}UdUd\theta \qquad (14)$$

Limits of integration for the variable $\theta$ become 0 and $2\pi$. Moreover, due to the symmetry with respect to the origin, the point $(U,\theta)$ has the same value as the point $(-U,\theta+\pi)$: we can therefore use the absolute value of $U$ to traverse the frequency plane and vary $\theta$ from 0 to $\pi$. We then get:

$$f(y,z) = \int_{0}^{\pi}\int_{-\infty}^{+\infty} P_\theta(U)e^{i2\pi Uu}|U|dUd\theta \qquad (15)$$

The internal integral represents the inverse Fourier transform of the Fourier transform of the projection, multiplied by the absolute value of $U$: this internal integral is a filtered projection $\hat{p}_\theta(u)$:

$$\hat{p}_\theta(u) = \int_{-\infty}^{+\infty} P_\theta(U)e^{i2\pi Uu}|U|dU \qquad (16)$$

It is therefore possible to reconstruct $f(x,y)$ by:

$$f(y,z) = \int_{0}^{\pi} \hat{p}_\theta(u)d\theta \qquad (17)$$

which is the back projection of filtered projections. The principle of filtered backprojection requires multiplying the Fourier transform of the projections by the absolute value of U, which is called the ramp filter. This filter sets the DC component to zero and therefore introduces negative values. The role of these negative values is to gradually erase the star artefacts left by other projections during the spreading operation.

### *4.3. Discretization problem*

In practice, the data are sampled with regard to the number of projections as well as the number of points per projection. Moreover, the image reconstructed in tomography is by nature a digital image, represented by its coordinates in a given basis. The continuous inversion formulas and operators presented above require some adaptation in order to be applied to the discrete case. It is thus necessary to define a discrete back-projection operator, which involves an approximation of the integral and interpolation models [29].

The "iradon" function (in Matlab) is used to calculate the inverse Radon transform of the Radon transform of $f(y,z)$. This function is an implementation of the discrete filtered backprojection algorithm. It takes as arguments, the matrix of projections, the angle theta of back-projections, the interpolation algorithm (linear interpolation in our case) used in the back-projection phase and the filter (Ram-Lak filter in our case) used to filter the projections.

## 5. Results of the 3D tomography reconstruction of a centrosymmetric particle with 120 angles of view and comparison with the 3D-shape obtained from 8 angles of view

### *5.1. 3D tomography reconstruction with 120 angles of view*

Using the 120 2D-projections reconstructed in section 3, we reconstruct the 3D-shape of the dendrite particle. The dimensions of the 2D-projection images are $680 \times 680$ pixels. We reconstruct thus 680 parallel horizontal slices (i.e. the number of lines of the selected part of each interferometric image) in order to reconstruct slice by

slice the 3D shape. The final 3D shape of the particle is obtained by stacking these 680 parallel horizontal reconstructed slices (see illustration in Fig. 6). A 2D-view of the reconstructed particle is presented in figure 8 (arbitrary projection). The 3D-shape reconstructed from 120 views is closed to the initial dendrite presented in figure 4. Visualization 2 shows the reconstructed particle from different angles of view. The main branches are clearly identifiable. The secondary branches (at the extremities of the six main branches) are less identifiable. We just observe compact blocks at the extremity of each main branch. The main branches of the 3D reconstruction are around 590 µm ($\pm 20\,\mu m$) long and 45 µm ($\pm 10\,\mu m$) wide, if we compare with the programmed particle (567 µm long and 37.8 µm wide), the dimensions are closed. The over-estimation of the size of the dendrite comes essentially from the threshold fixed to calculate the new support at each iteration [21]. Even if some of the 2D shapes reconstructed with the phase retrieval algorithm are less precise, the combination of the 120 views enables a 3D-reconstruction with more details. The ER algorithm takes between ten seconds and one minute for one reconstruction (depending on the portable computer used, and on the number of iterations chosen). Here, we use a computer with a processor Intel Core i7-8850H @2.60GHz. The 120 reconstructions require between twenty minutes (using 3 iterations) and two hours (using 10 iterations). Once the 120 reconstructions are done, the tomographic reconstruction takes two minutes to compute the 3D-shape of the particle.

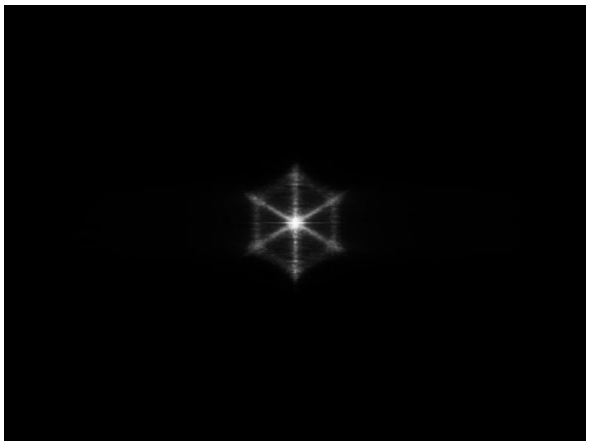

Fig. 8. 3D shape visualization of the dendrite created from 120 angles of view (see visualization 2)

*5.2. Comparison with the 3D-shape obtained from 8 angles of view*

In practice, it seams impossible to synchronize 120 sensors all around the region of interest. In this subsection a 3D reconstruction is done using only 8 angles of view (we take thus into account only eight views of the 120 2D-reconstructions of figure 5, those corresponding to a rotation angle of 45° between two successive angles of view) in order to be as close as possible to a potential experimental study that could be done in a configuration with eight cameras. A 3D-shape is obtained from the 2D reconstructions of the 8 angles of view. A 2D-view of the reconstructed particle is presented in figure 9 (projection in the plane of the main face of the dendrite). Visualization 3 shows the reconstructed particle from different angles of view. Compared to the 3D-shape reconstructed with 120 angles of view, the dimensions of the main branches is still 590 µm ($\pm 20\,\mu m$) long and 45 µm ($\pm 10\,\mu m$) wide but the separations between these branches are more blurred. Noise is visible around the particle due to the artifact caused by the lack of angles of view. The increase in the number of views makes it possible to refine the 3D shape obtained and reduce the noise. However, we observed that even if the reconstruction is more noisy, it remains remarkable and promising to perform a well accuracy tomography of the centrosymmetric particles using interferometric imaging.

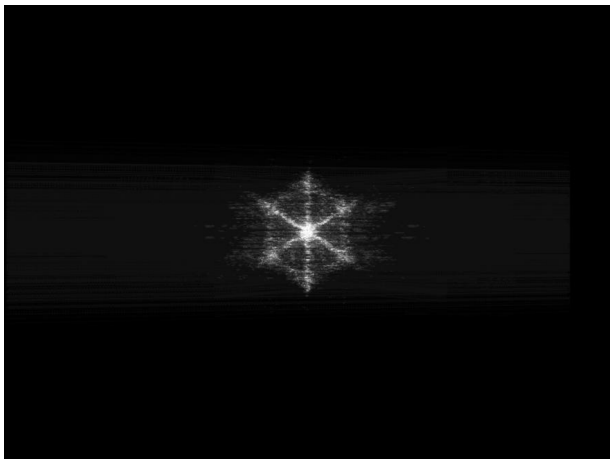

Fig. 9. 3D shape visualization of the dendrite created from 8 angles of view (see visualization 3)

## 6. Results of the 3D tomography reconstruction for a non-centrosymmetric particle obtained from 120 and 15 angles of view.

The particle that is now considered is a reverse Y-like rough particle, this shape is non-centrosymmetric. The reversed Y-shaped particle that is now considered is depicted on Figure 10. It is made of 1500 on-state micromirrors randomly located over the entire surface of the particle. It consists of three main branches, each being 652 µm long and 30 µm wide that make an angle of 120° two by two.

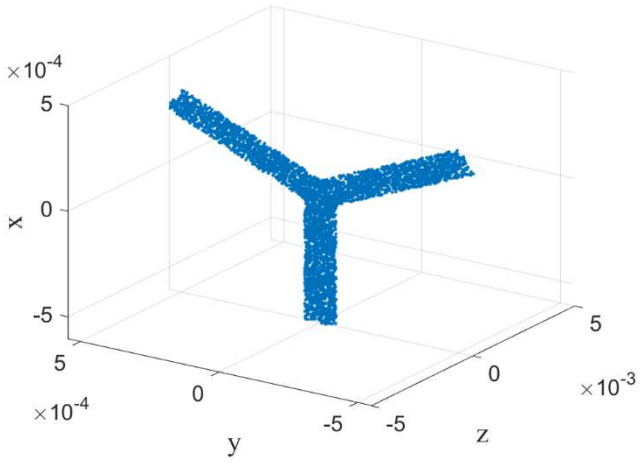


Fig. 10. Three-dimensional representation of reversed Y-like particle that will be considered. (All axes in meters)

The principle is the same that for the previous particle. The individual 2D-reconstructions are done for the 120 views using the error-reduction algorithm and the final 3D reconstruction using the filtered backprojection. Two 3D-reconstruction are done, one with the 120 views at 3° from each other, a 2D-view of the reconstructed particle is presented in figure 11 (arbitrary projection) and the second one with only 15 views at 24° from each other (see Fig. 12.). Visualizations 4 and 5 show respectively the reconstructed particle from different angles of view using 120 and 15 angles of view respectively. The three branches of the reversed Y-like particle is clearly identifiable on the first visualization. On the second visualization, noise is visible around the branches as for the 3D reconstruction of the dendrite but the three branches are clearly identifiable. We also observed the birth of what appears to be a fourth branch between the two lower branches in the two 3D-reconstructions. This branch is probably a piece of the twin image [21] of the reversed Y. It is only seen very weakly because it is not present in all 2D-reconstructions. In conclusion, the 3D tomographic reconstruction for non-centrosymmetric particles remains promising for an experimental work even if the numbers of cameras has to be more important.

Fig. 11. 3D shape visualization of the Y particle created from 120 angles of view (see visualization 4)

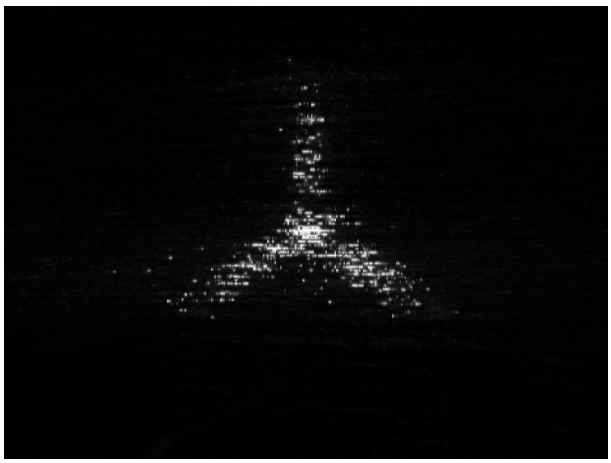

Fig. 12. 3D shape visualization of the Y particle created from 15 angles of view (see visualization 5)

Before to conclude, let us try to identify some difficulties that could occur in a real set-up.

First, in a real configuration, we can suspect that a unique direction of illumination would not be enough for any kind of particle. In particular in the case of opaque rough particles, auto-shadowed areas could be produced, as already observed with ashes [16]. The use of multiple directions of illumination would be probably necessary.

Second, the different images of a particle would not be perfectly centered. In a real image, the interferometric image of one particle has first to be identified, isolated and cropped for each angle of view. At this stage of our study, the image processing applied to these selected parts of the images recovers the center of the speckle patterns before each 2D-reconstruction. Afterwards, all 2D-reconstructions are centered again before the filtered back-projection and the 3D-reconstruction. A correct 3D-reconstruction is thus ensured. Nevertheless, a non-centered position of the particle in the field of view would induce an uncertainty in the exact knowledge of each angle of view (limited to the field of view of the imaging set-up). A limitation of the accuracy of the 3D-reconstruction is thus expected. It will be studied in more detail in the future.

One can further wonder what would happen if two particles were present in the region of interest. Different cases could occur:

- the interferograms of the two particles never overlap (for all angles of view). The 3D-reconstruction of both particles could then be done separately, as explained in this article.

- The interferograms overlap for all angles of view. Some methods, based on reference [29] could be proposed to perform the 2D-reconstructions of both particles. Nevertheless, preliminary studies show that the twin image problem, already encountered with one particle using the ER-algorithm, has to be solved in the case of a pair of particles.
- The interferograms overlap for some angles of view and not for the others: it would lead to a very complex procedure of reconstruction that has not been established now.

It will be interesting in the future to study the solutions that would propose a deep learning approach [31,32]

## 7. Conclusion

The 3D-tomography of irregular particles in a flow would be of great interest in many domains as meteorology, aircraft safety, environmental research, health, biology, nuclear safety. In 3D-tomography, the acquisition of many angles of view, requires specific set-ups. However, contrary to medicine where the patient is motionless, as in a CT-scan, particles are moving fast in a flow. A single-shot technique, with synchronized sensors disseminated around the particle appears necessary. Interferometric particle imaging is a potential candidate to develop such systems. But different difficulties have to be solved. First, in this case, the images that are recorded do not give the particle's shape directly, but its 2D-autocorrrelation. Reconstruction methods are thus required. In these conditions, the possibility to perform accurate 3D-reconstructions from different views is not obvious and has to be demonstrated using simplified set-ups. We have shown in previous studies that a Digital Micromirror Device (DMD) can be used to reproduce artificially the interferometric images that would be given by a real rough particle. Such a set-up offers the opportunity to test the feasibility of 3D-particle's tomography from a wide number of interferometric images of the same particle with different angles of view, at a low cost. In the present paper we have shown that an accurate 3D-reconstruction of a "programmed" rough particle can be done from a set of 120 interferometric images, as in a CT-scan configuration, with an angular separation of 3° between two views. Different steps are necessary:

- the production of 120 interferometric images of the same particle from different angles of view. This has been done with synthetic particles "programmed" with a DMD.
- for each of these 120 views, the reconstruction of the 2D-projection of the particle from the corresponding interferometric image using a phase retrieval algorithm (the error-reduction (ER) algorithm in this study).
- The 3D-reconstruction of the particle from the 120 2D-projections obtained in previous step. The filtered back projection is used for this step of tomographic reconstruction. It requires multiplying the Fourier transform of the 2D-projections by a filter ramp before back projection.

The method has been first tested on a dendrite-like rough particle (centrosymmetric image) and then on a reverse Y-like rough particle (non-centrosymmetric shape). The case of non-centrosymmetric shapes is more complex because the reconstruction of each 2D-projection using the ER-algorithm suffers the twin-image problem that has to be solved. Our results show the possibility to perform an accurate quantitative 3D-reconstruction of these particles from the acquisition of 120 interferometric images.

In the perspective of a simplified configuration that would require less angles of view, the same procedure has been tested considering only 8 or 15 angles of view, regularly chosen around the particle. The 3D-reconstruction of the particles has been shown to be less precise and more noisy, but still well accurate. This study demonstrates the potentiality of interferometric particle imaging to perform the 3D-tomography of rough particles in a flow, considering only a relatively low number of angles of view (between 8 and 15).

Nevertheless, different aspects need to be addressed in the future to identify and solve some possible limitations: the use of different directions of illumination in the case of opaque particles that could produce auto-shadowed areas using only one illumination direction; the 3D-reconstruction of neighbored particles whose interferometric images overlap completely or partially; the description of sources of noise as the influence of the exact 3D-position of the particle in the volume of interest. Deep learning methods [31, 32] can probably offer very interesting solutions to some of these problems that will be addressed in future works. With an expansion of the data set with more complex shapes to train the network, the method seems indeed interesting to improve the convergence of the reconstruction and to deal with the sources of noise.

## 8. References


[1] U. S. Kamilov, I. N. Papadopoulos, M. H. Shoreh, A. Goy, C. Vonesch, M. Unser, and D. Psaltis. Optical Tomographic Image Reconstruction Based on Beam Propagation and Sparse Regularization. IEEE Transactions on Computational Imaging 2(1), 59–70 (2016).

[2] T-A. Pham, E. Soubies, A. Goy, J. Lim, F. Soulez, D. Psaltis, and M. Unser. Versatile reconstruction framework for diffraction tomography with intensity measurements and multiple scattering. Opt. Express 26(3), 2749–2763 (2018).

[3] J. Bailleul, B. Simon, M. Debailleul, L. Foucault, N. Verrier, and O. Haeberlé. Tomographic diffractive microscopy: Towards high-resolution 3-D real-time data acquisition, image reconstruction and display of unlabeled samples. Opt. Commun. 422, 28–37 (2018)

[4] A. Berdeu, F. Momey, B. Laperrousaz, T. Bordy, X. Gidrol, J-M. Dinten, N. Picollet-D'hahan, and C. Allier. Comparative study of fully three-dimensional reconstruction algorithms for lens-free microscopy. Appl. Opt. 56(13), 3939–3951 (2017).

[5] M. J. Berg, and G. Videen, Digital holographic imaging of aerosol particles in flight, J. Quant. Spectrosc. Radiat. Transfer 112, 1776-1783 (2011).

[6] M. Brunel, B. Delestre, and M. Talbi, 3D-reconstructions for the estimation of ice particle's volume using a two-views interferometric out-of-focus imaging set-up, Review of Scientific Instruments 90, 053109 (2019)

[7] G. König, K. Anders, A. Frohn, A new light-scattering technique to measure the diameter of periodically generated moving droplets, J.of Aerosol Sci. 17 (1986) 157-167.

[8] R. Ragucci, A. Cavaliere, P. Massoli, Drop sizing by laser light scattering exploiting intensity angular oscillation in the Mie regime, Part. Part. Syst. Charact. 7 (1990) 221–225.

[9] A.R. Glover, S.M. Skippon, R.D. Boyle, Interferometric laser imaging for droplet sizing: a method for droplet-size measurement in sparse spray systems, Appl. Opt. 34 (1995) 8409–8421.

[10] H.E. Albrecht, M. Borys, N. Damaschke, C. Tropea, Laser Doppler and Phase Doppler Measurement Techniques, Springer Verlag, Berlin, 2003.

[11] D. Sugimoto, K. Kawaguchi, T. Kawaguchi, K. Matsuura, Y. Hardalupas, A. Taylor, K. Hishida, Extension of the compressed interferometric particle sizing technique for three-component velocity measurements, (2006).

[12] J. Jacquot Kielar, P. Lemaitre, C. Gobin, Y. Wu, E. Porcheron, S. Coëtmellec, G. Gréhan, and M. Brunel, Simultaneous interferometric in-focus and out-of-focus imaging of ice crystals, Opt. Commun. 372, 185–195 (2016).

[13] M. Brunel, S. Gonzalez Ruiz, J. Jacquot, and J. van Beeck, On the morphology of irregular rough particles from the analysis of speckle-like interferometric out-of-focus images, Opt. Commun. 338, 193–198 (2015).

[14] L. Ouldarbi, M. Talbi, S. Coëtmellec, D. Lebrun, G. Gréhan, G. Perret, and M. Brunel, 3D-shape recognition and size measurement of irregular rough particles using multi-views interferometric out-of-focus imaging, Appl. Opt. 55, 9154-9159 (2016).

[15] M. Talbi, G. Gréhan, M. Brunel, Interferometric particle imaging of ice particles using a multi-view optical system, Appli. Opt. 57, 6188-6197 (2018).

[16] S.G. Ruiz, J. van Beeck, Sizing of sand and ash particles using their speckle pattern: influence of particle opacity, Exp. Fluids 58 (2017) 100–108.

[17] Y. Wu, Y. Gong, L. Shi, Z. Lin, X. Wu, C. Gong, Z. Zhou, Y. Zhang, Backward interferometric speckle imaging for evaluating size and morphology of irregular coal particles, Opt. Commun. 491 (2021) 126957.

[18] J. Sun, H. Zhang, W. Fan, and S. Chen, Comparison of aspect ratios of ellipsoidal particles through interferometric out-of-focus images, J. Opt. Soc. Am. A 38, 395-400 (2021).

[19] M. Fromager, K. Aït Ameur, and M. Brunel, "Digital micromirror device as programmable rough particle in interferometric particle imaging," Appl. Opt. 56, 3594-3598 (2017)

[20] D. Leroy, E. Fontaine, A. Schwarzenboeck, J. W. Strapp, A. Korolev, et al.. Ice crystal sizes in high ice water content clouds. Part 2: Statistics of mass diameter percentiles intropical convection observed during the HAIC/HIWC project, J. of Atmos. and Ocean.Technol., 34 (2017) 117-136.

[21] B. Delestre, A. Abad, M. Talbi, M. Fromager, M. Brunel, Experimental particle's shapes reconstructions from their interferometric images using the Error-Reduction algorithm, Optics Communications, Volume 498, 2021, 127229.

[22] J. R. Fienup, Phase retrieval algorithms: a comparison, Appl. Opt. 21, 2758-2769 (1982)

[23] J. N. Cederquist, J. R. Fienup, J. C. Marron, and R. G. Paxman, Phase retrieval from experimental far-field speckle data, Opt. Lett. 13, 619-621 (1988).

[24] H. Shen, L. Wu, Y. Li, and W. Wang, Two-dimensional shape retrieval from the interferometric out-of-focus image of a nonspherical particle - Part I: theory, Appl. Opt. 57, 4968-4976 (2018).

[25] R. Fienup, T.R. Crimmins and W. Holsztynski, Reconstruction of the support of an object from the support of its autocorrelation, J. Opt. Soc. Am. 7 3-13 (1982).

[26] Herman, G. T., Fundamentals of computerized tomography: Image reconstruction from projection, 2nd edition, Springer, 2009

[27] Kak, A. C., and M. Slaney, Principles of Computerized Tomographic Imaging, New York, NY, IEEE Press, 1988.

[28] F. Dubois, Reconstruction des images tomographiques par rétroprojection filtrée, ACOMEN, volume 4, n°2, 1998, pages 92-99.

[29] M. Brunel, P. Lemaitre, E. Porcheron, S. Coëtmellec, G. Gréhan, J. Jacquot-Kielar, "Interferometric out-of-focus imaging of ice particles with overlapping images", Appl. Opt. 55 (2016) 4902-4909.

[30] P.M. Joseph, R.D. Spital, C.D. Stockham, The effect of sampling in CT images, Computed Tomography, 1980, vol. 4, p. 189-206.

[31] H. Zhang, Z. Li, J. Sun, Y. Fu, D. Jia, T. Liu, Characterization of particle size and shape by an IPI system through deep learning, Journal of Quantitative Spectroscopy and Radiative Transfer, Volume 268, 2021, 107642.

[32] P. Piedra, A. Kalume, E. Zubko, D. Mackowski, Y. Pan, G. Videen, Particle-shape classification using light scattering: An exercise in deep learning, J. Quant. Spectrosc. Radiat. Transfer 231 (2019) 140-156